

Grafting Charged Species to Membrane-Embedded Scaffolds Dramatically Increases the Rate of Bilayer Flipping

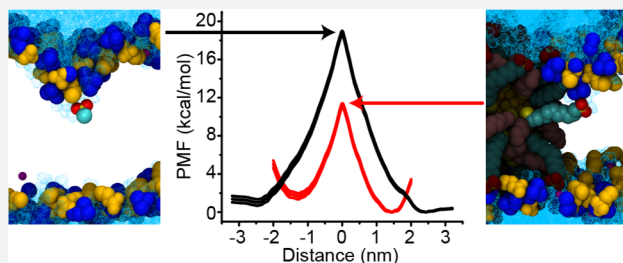
Reid C. Van Lehn^{*,†} and Alfredo Alexander-Katz[‡]

[†]Department of Chemical and Biological Engineering, University of Wisconsin—Madison, Madison, Wisconsin 53706, United States

[‡]Department of Materials Science and Engineering, Massachusetts Institute of Technology, Cambridge, Massachusetts 02139, United States

S Supporting Information

ABSTRACT: The cell membrane is a barrier to the passive diffusion of charged molecules due to the chemical properties of the lipid bilayer. Surprisingly, recent experiments have identified processes in which synthetic and biological charged species directly transfer across lipid bilayers on biologically relevant time scales. In particular, amphiphilic nanoparticles have been shown to insert into lipid bilayers, requiring the transport of charged species across the bilayer. The molecular factors facilitating this rapid insertion process remain unknown. In this work, we use atomistic molecular dynamics simulations to calculate the free energy barrier associated with “flipping” charged species across a lipid bilayer for species that are grafted to a membrane-embedded scaffold, such as a membrane-embedded nanoparticle. We find that the free energy barrier for flipping a grafted ligand can be over 7 kcal/mol lower than the barrier for translocating an isolated, equivalent ion, yielding a 5 order of magnitude decrease in the corresponding flipping time scale. Similar results are found for flipping charged species grafted to either nanoparticle or protein scaffolds. These results reveal new mechanistic insight into the flipping of charged macromolecular components that might play an important, yet overlooked, role in signaling and charge transport in biological settings. Furthermore, our results suggest guidelines for the design of synthetic materials capable of rapidly flipping charged moieties across the cell membrane.



1. INTRODUCTION

The cell membrane is the biological interface that divides the cell interior from its external environment. The membrane contains amphiphilic lipids that self-assemble into a characteristic bilayer morphology in which a hydrophobic core region composed of lipid tails is sandwiched between two hydrophilic regions composed of solvated lipid heads. A primary function of the membrane is to control extracellular transport, which is possible due to the barrier presented by the hydrophobic bilayer core to the passive diffusion of soluble material.¹ Charged and hydrophilic small molecules are instead actively transported across the membrane in highly regulated processes. Identifying methods to bypass these transport processes and translocate material directly across the membrane could eliminate bottlenecks in the delivery of soluble synthetic molecules, such as drugs or imaging agents, to the cell interior.^{2,3} Achieving this goal requires a molecular understanding of the barrier presented by the bilayer to the passive diffusion of soluble, and particularly charged, molecules.

The translocation of charged molecules across lipid bilayers is typically described by the solubility–diffusion model,¹ which posits that the charged species must dissolve in the bilayer core where the 40-fold decrease of the dielectric constant relative to bulk water leads to a large (≈ 50 kcal/mol⁴) barrier to translocation. In contrast, molecular simulations have found

that the free energy barrier for charge translocation emerges from lipid deformations that allow a charged species to cross the bilayer while maintaining its solvation shell.^{4–7} Simulations have estimated this barrier as ≈ 20 kcal/mol, which is in better agreement with experimental measurements of ion permeability.⁶ Nonetheless, the time scale associated with charge translocation is still estimated as hours to days,⁶ which is too slow to be relevant to most biological processes.

Despite these past findings, recent experiments have suggested that charged components of complex biological macromolecules can cross lipid bilayers much more rapidly than expected.⁸ For example, the post-translational movement of charged loops across the bilayer is an essential step in the biogenesis of the membrane protein aquaporin-1.^{9,10} A similar process dictates the topology of the protein EmrE.^{11–13} Perhaps most surprising is that multiple charged loops of the multispanning membrane protein LacY cross the bilayer within seconds following a change in lipid composition,^{14,15} even in the absence of transmembrane protein transporters.¹⁶

In addition to these biological examples, it was recently found that small gold nanoparticles (NPs) protected by anionic, amphiphilic surface monolayers enter cells even with

Received: November 29, 2016

Published: February 24, 2017

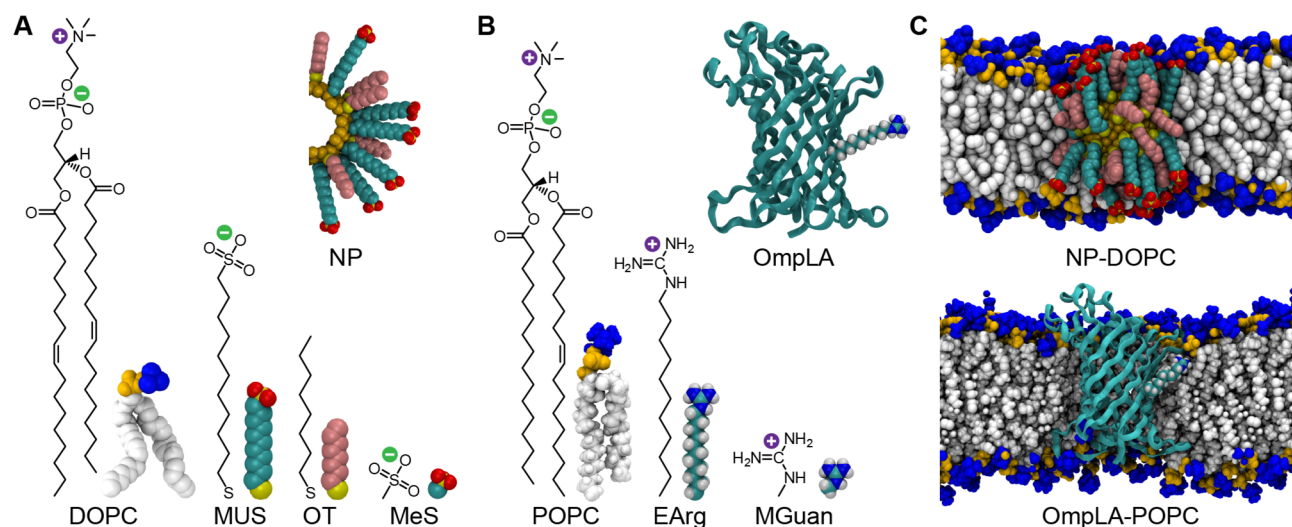


Figure 1. Chemical structures and simulation snapshots of systems studied. (A) Structures and corresponding snapshots of the lipid DOPC, end-functionalized anionic ligand MUS, hydrophobic ligand OT, and small-molecule analogue MeS, simulated at united-atom resolution. A NP grafted with MUS and OT in a 1:1 ratio is illustrated. Lipid phosphate groups are drawn in yellow and choline groups in blue. (B) Structures and corresponding snapshots of the lipid POPC, cationic extended arginine variant EArg, and small-molecule analogue MGuan, simulated at all-atom resolution. The β -barrel protein OmpLA with a central alanine residue mutated to EArg is illustrated. (C) Snapshots of the NP embedded in a DOPC bilayer (NP-DOPC, top) and OmpLA embedded in a POPC bilayer (OmpLA-POPC, bottom) after 50 ns of unbiased equilibration. Water, ions, and protein side chains are not illustrated.

endocytosis inhibited.¹⁷ Internalization does not lead to cell death or trigger the leakage of a membrane impermeable dye,¹⁷ suggesting that a large number of charged groups cross the membrane without inducing large membrane defects. Despite a high surface charge density, the NPs also insert into several model membrane systems,^{18–21} with stable insertion correlating with an increase in nonendocytic uptake.¹⁸ Experimental studies of similar monolayer-protected NPs have observed behavior consistent with bilayer insertion in several other systems.^{22–24} Because bilayer insertion requires charged ligand end groups to cross the bilayer, these observations again indicate that charged groups may cross the bilayer more rapidly than anticipated when grafted to a complex material system, although the molecular details of this process are unknown. Understanding how such grafting affects the rate of charge transport could be of great use in drug delivery applications by revealing design guidelines for synthetic materials capable of ferrying water-soluble therapeutic compounds or genetic material across the cell membrane. This understanding may also reveal new signaling pathways or charge regulation mechanisms in biological systems.

In this work, we use atomistic molecular dynamics simulations to investigate the “flipping” of charged species across a homogeneous lipid bilayer. We define flipping as the movement of a charged species across the bilayer when it is grafted to the surface of a membrane-embedded scaffold and cannot fully translocate to bulk solvent. The iterative flipping of charged species could facilitate the transport of charged macromolecules across the bilayer without having to simultaneously translocate large numbers of charges; however, even flipping a single charged species could still occur too slowly to explain experimental observations. We first calculate the rate with which a charged ligand flips across the membrane when grafted to the surface of a small (<5 nm in diameter, with a core diameter smaller than the thickness of the bilayer) membrane-embedded NP. We find that the free energy barrier for flipping a NP-grafted ligand is significantly lower than the barrier for

translocating an isolated small-molecule analogue of the ligand end group, allowing flipping to occur on biologically relevant time scales. The flipping barrier is reduced because the grafted ligand is unable to reach favorable, well-solvated positions in bulk water. We further compute the flipping energy barrier and time scale for an engineered variant of arginine attached to a β -barrel protein, and again find that the barrier is lower than the barrier for translocating an isolated small-molecule analogue. Together, these results suggest a general mechanism by which charged species grafted to membrane-embedded scaffolds flip across lipid bilayers several orders of magnitude faster than previously anticipated.

2. RESULTS

2.1. Description of Simulated Systems. Atomistic molecular dynamics simulations are performed to calculate the free energy barrier for flipping or translocating various charged species across single-component lipid bilayers. Four systems (summarized in Figure 1, with components listed in Table S1) are simulated in order to compare the barrier for flipping a charged species that is grafted to a membrane-embedded scaffold to the barrier for translocating an isolated small molecule.

The first system consists of a mixed-monolayer-protected gold nanoparticle embedded within a dioleoylphosphatidylcholine (DOPC) bilayer; this is referred to as the NP-DOPC system (Figure 1C). DOPC is a zwitterionic, unsaturated lipid representative of lipids in the plasma membrane. Two ligands are grafted in a 1:1 ratio to the NP surface: 1-mercaptopundecanesulfonate (MUS) and octanethiol (OT). MUS has an 11-carbon alkane backbone that is end-functionalized with an anionic sulfonate moiety, while OT has an eight-carbon alkane backbone (Figure 1A). The second system consists of an isolated methylsulfonate (MeS) group in the presence of a DOPC bilayer; this is referred to as the MeS-DOPC system. MeS is a small-molecule analogue to the MUS sulfonate end group and provides a suitable comparison to

previous simulations of ion translocation.^{5–7} The third system consists of the bacterial transporter OmpLA (PDB ID: 1QDS) embedded within a POPC lipid bilayer; this is referred to as the OmpLA-POPC system (Figure 1C). POPC is a zwitterionic lipid, similar to DOPC, that is abundant in bacterial membranes. A central alanine residue at position 210 in the OmpLA primary sequence is mutated to a cationic extended arginine variant (EArg) in which an additional 8 methylene groups are inserted prior to the guanidinium end group of the arginine chain (Figure 1B). This position is chosen because it is near the bilayer midplane and has been previously mutated to calculate water–membrane transfer free energies.^{25–27} The final system consists of an isolated methylguanidium (MGuan) group in the presence of a POPC bilayer; this is referred to as the MGuan-POPC system. MGuan is a small-molecule analogue to the EArg end group.

2.2. The Free Energy Barrier for Flipping NP-Grafted MUS Is Significantly Lower than the Barrier for Translocating Isolated MeS. To calculate the free energy barrier for flipping a charged, NP-grafted ligand across a lipid bilayer, the potential of mean force (PMF) is calculated from umbrella sampling simulations as detailed in Methods. Two PMFs are calculated: (i) the PMF for flipping a single NP-grafted MUS ligand and (ii) the PMF for translocating an isolated MeS group. The initial NP-DOPC system configuration is selected to have a nearly equal number of MUS ligands on either side of the bilayer to achieve similar configurations before and after flipping a single ligand (Figure S1). The MeS-DOPC system allows the barrier for isolated ion translocation to be compared to the flipping of a NP-grafted MUS ligand.

Figure 2A compares the two PMFs as a function of the distance, projected onto the z -axis, between the center-of-mass of the lipid bilayer and the sulfur atom in the sulfonate group (denoted by d_z). As expected, both PMFs are approximately symmetric with respect to the bilayer midplane ($d_z = 0$); the small difference of 1–2 kcal/mol between the two minima on either side of the bilayer is consistent with prior studies.²⁸ The shape and magnitude of the MeS PMF agree well with previous studies of single ion translocation.⁶ The MUS PMF has the same features, including a maximum for $d_z = 0$, as the MeS PMF (illustrated via the shifted MUS PMF indicated by a dashed red line in Figure 2A). The MUS PMF increases at $d_z \approx \pm 1.5$ nm because the grafted ligand is fully extended at these distances, as shown in Figure 2B; reaching larger values of d_z requires the displacement of the entire NP. The major difference between the two profiles is the barrier for flipping, ΔG_{flip} , which is estimated as the difference between the maximum of the PMF and the minimum of the PMF for $d_z > 0$; ΔG_{flip} is used to refer to both the barrier for flipping a grafted species and the barrier for translocating an isolated species. ΔG_{flip} is approximately 18.8 kcal/mol for MeS; in comparison, ΔG_{flip} decreases to only 11.2 kcal/mol for MUS (Table 1). Because MeS and the MUS end group are chemically identical, the PMFs confirm that grafting the charged species to the membrane-embedded NP scaffold significantly decreases the free energy barrier for flipping relative to the free energy barrier for single-ion translocation.

It should be noted that while the barrier for flipping MUS is dramatically reduced, it is still large compared to the barriers for translocating polar, but uncharged, small molecules. For example, the translocation free energy barrier has been measured as 5–6 kcal/mol for water,^{29,30} 5–7 kcal/mol for

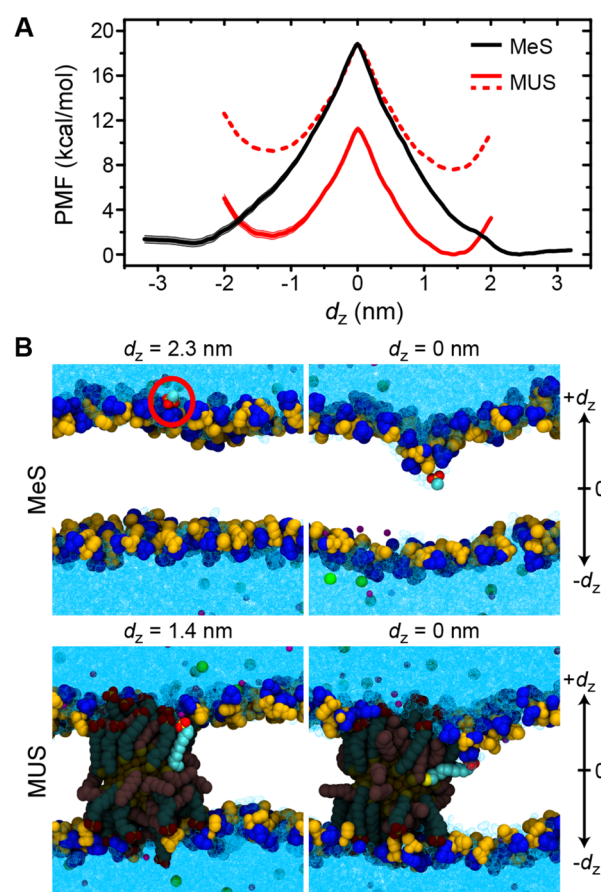


Figure 2. Free energy cost for translocating MeS and flipping MUS across the bilayer. (A) PMFs for translocating an isolated MeS molecule (black) and flipping a single NP-grafted MUS ligand (red) as a function of d_z . Each PMF curve is offset such that its minimum value for $d_z \gg 0.0$ is set to zero. For comparison, the MUS PMF is also shifted such that its maximum coincides with the maximum of the MeS PMF (dashed red line). The error is shown as the shaded region around each solid line. (B) Representative snapshots of the configurations at the minimum (for $d_z \gg 0$) and maximum (for $d_z = 0$) of both PMFs. Water is shown in cyan, sodium ions are in purple, and chloride ions are in green; lipid tails are not drawn. The flipped ligand is highlighted in the MUS snapshots.

Table 1. Parameters To Estimate the Flipping/Translocation Time Scale (τ_{flip})^a

	ΔG_{flip} (kcal/mol)	k_d^{-1} (ns)	τ_{flip} (s)
MeS	18.8	6.8 ± 1.3	2.4×10^5
MUS	11.2	7.2 ± 0.9	1.1
MGuan	14.4	3.5 ± 0.4	98.9
EArg ($d_z > 0$)	12.2	10.4 ± 1.8	8.3
EArg ($d_z < 0$)	7.2	17.4 ± 3.2	4.1×10^{-3}

^a ΔG_{flip} is determined from the PMFs (Figure 2 and Figure 5). k_d^{-1} is estimated from relaxation simulations (example trajectories in Figure 4 and Figure S4); the standard error is provided. τ_{flip} is calculated from eq 1 and eq 2.

cholesterol,³¹ and 3–6 kcal/mol for polar amino acid side chains.³² These comparisons emphasize that the measured flipping free energy barrier is physically reasonable, as it is expected that a charged species would have a larger free energy barrier than an uncharged small molecule.

2.3. MeS and NP-Grafted MUS Induce Local Bilayer Defects. Analysis of the US trajectories provides insight into the molecular mechanism, and in particular the role of lipid deformations, in order to understand the differences between the two PMFs shown in Figure 2. In prior computational studies of single-ion translocation, two types of deformation have been observed: the translocating ion either stabilizes the formation of a membrane-spanning, water-filled pore that enables passive diffusion across the bilayer, or the ion locally perturbs lipids within a single bilayer leaflet to maintain its solvation shell.⁶ The simulation snapshots in Figure 2 suggest that lipids deform without forming a membrane-spanning pore, consistent with the latter, local defect model.

Figure 3A illustrates the lipid deformations shown in Figure 2 by plotting the number density of all atoms in polar groups

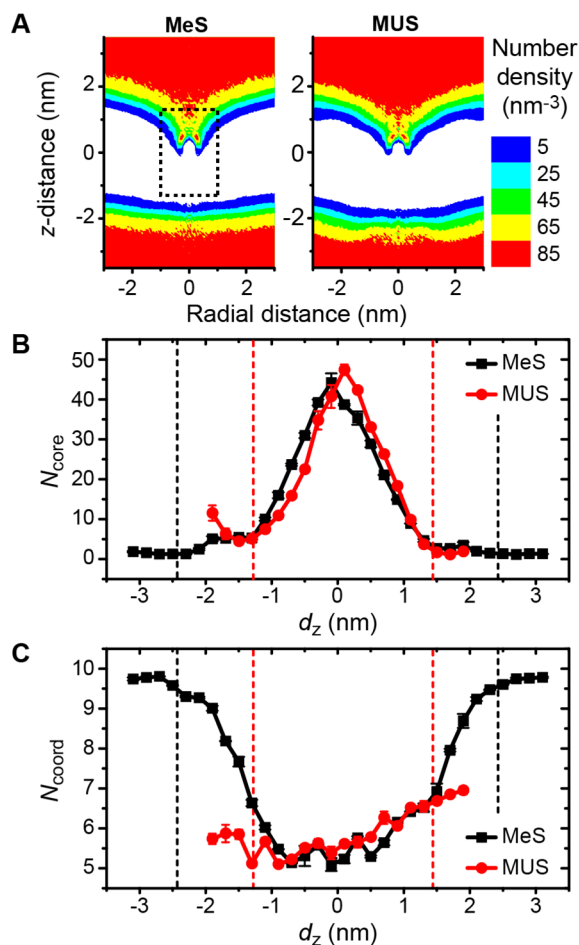


Figure 3. Analysis of charge-induced bilayer deformations. (A) Number density of all atoms in polar groups within a cylinder centered on either the MUS end group or MeS, time-averaged from the US trajectories in which each species is held at $d_z = 0$ and deforms the upper bilayer interface. Densities are averaged radially due to the cylindrical symmetry; negative values of the radial distance are identical to the corresponding positive values and are included for visual clarity. (B) N_{core} , the number of polar groups that penetrate into the bilayer core near the charged species (within the dashed box in panel A). Dashed lines indicate the minima of the MeS (black) and MUS (red) PMFs from Figure 2A. Error bars present the standard error calculated by splitting the US trajectory into three 20 ns blocks. See the Supporting Information for further details on the calculation. (C) N_{coord} , the number of polar groups coordinating each species. Dashed lines and error bars are defined in panel B.

(including water molecules, ions, lipid head groups, and ligand end groups) within a cylinder centered on either the charged MeS ion (left) or MUS end group (right); also see Figure S2 for additional density profiles centered on the NP. Each profile is calculated from the US trajectory in which the species is restrained to $d_z = 0$ and deforms the upper bilayer leaflet. The profiles for MeS and MUS are very similar. In each case, lipids deform to allow water and other polar molecules to coordinate the charged species, despite its position near the bilayer midplane (see snapshots in Figure 2B). Both density profiles are consistent with the local deformation of a single bilayer leaflet as opposed to the formation of a membrane-spanning pore.

Figure 3B quantifies lipid deformations as a function of d_z via the core number, N_{core} , which reports on the penetration of polar groups into the bilayer core region.⁶ N_{core} is defined as the number of polar groups that have central atoms within a radial distance of 1.0 nm from the central sulfur atom of the charged species (measured in the x - y plane) and within 1.3 nm of the bilayer midplane (measured along the z -axis); this region is indicated by the dashed box in Figure 3A. Consistent with the density profiles in Figure 3A, N_{core} is similar for both MeS and MUS for all values of d_z . N_{core} reaches a maximum for a value of $d_z = 0$ due to local defect formation and then decreases to nearly zero near the bilayer interface when the bilayer core is unperturbed. The dashed vertical lines indicate the positions of the minima for the PMFs from Figure 2A to emphasize that the increase in N_{core} coincides with the increase in the MUS PMF, which is likely dominated by the cost of bilayer deformation, but does not fully explain the increase in the MeS PMF. Because both charged species deform the bilayer to a similar extent, this deformation likely contributes similar entropic and enthalpic membrane-related free energy contributions to ΔG_{flip} , requiring a different explanation for the difference in the PMFs shown in Figure 2B.

2.4. Reduced Access to Water Lowers the Free Energy Barrier for MUS Flipping. The similarity in the lipid deformations induced by both MeS and MUS does not explain the relative magnitudes of ΔG_{flip} (Figure 2). However, a difference between the two species is the change in the coordination number, N_{coord} , as each species crosses the bilayer. N_{coord} is defined as the number of polar groups that have central atoms within a threshold distance equal to the position of the first minimum of the radial distribution function corresponding to each group (see Figure S3 and Table S2). Figure 3C presents N_{coord} as a function of d_z as calculated from the US trajectories. N_{coord} decreases for MeS as the ion moves from a highly solvated region, where the PMF is near its minimum value (Figure 2), toward the bilayer midplane, reflecting the partial dehydration of the ion.⁶ In contrast, N_{coord} for the MUS end group is nearly constant between the values of d_z that correspond to the two minima of the MUS PMF (dashed vertical lines), although it is still similar to N_{coord} for MeS.

The N_{coord} comparison indicates that both MeS and the MUS end group experience similar solvation environments as a function of d_z ; however, the attachment of the MUS ligand to the NP restricts the position of the end group to values of d_z for which its coordination shell is decreased. The decreased coordination shell unfavorably reduces the effective dielectric constant near the ion and increases the translocation energy.⁶ This difference explains the low value of ΔG_{flip} for MUS relative to MeS: ΔG_{flip} for MeS arises from both lipid deformations and the partial removal of its coordination shell relative to a

favorable position in bulk water, while ΔG_{flip} for MUS is due primarily to lipid deformations. The results of Figure 3 thus illustrate that MUS flipping is similar to the translocation of typical ions, but has a much lower free energy barrier because grafting to the NP core prevents the end group from reaching highly solvated configurations, effectively destabilizing the states corresponding to free energy minima.

2.5. NP-Grafted MUS Flips across the Bilayer on Physiologically Relevant Time Scales. The large decrease in ΔG_{flip} for a NP-anchored MUS end group relative to an isolated MeS molecule suggests that the corresponding flipping time scale, τ_{flip} , should also significantly decrease relative to the time scale for MeS translocation. Assuming that the rate-limiting step in flipping and translocation is the time necessary for the charged species to reach the center of the bilayer, τ_{flip} can be estimated by adapting an approach used to estimate the time scale for lipid flip-flop.^{31,33,34} The rate with which a single charged species reaches the bilayer center, k_f , is related to ΔG_{flip} by

$$k_f = k_d \exp(-\Delta G_{\text{flip}}/kT) \quad (1)$$

where k_d is the rate with which the charged species relaxes to a local free energy minimum. A complete flip requires the species to first reach the bilayer center and then relax to the opposite interface. As there is an equal likelihood of relaxing to either interface from the bilayer center, the total flipping rate is^{31,33,34}

$$k_{\text{flip}} = \frac{1}{2} \frac{1}{k_f^{-1} + k_d^{-1}} = \tau_{\text{flip}}^{-1} \quad (2)$$

To approximate k_d^{-1} , simulations are initialized from configurations extracted from the US trajectories for which $d_z \approx 0$. Unbiased simulations are performed for both MeS and MUS starting from 20 distinct configurations (10 configurations in which the upper leaflet deforms and 10 configurations in which the lower leaflet deforms) for a total of 40 simulations. The time necessary for the species to relax to a value of d_z corresponding to a local minimum in the PMF (Figure 2) is measured for each trajectory; k_d^{-1} is estimated for each species as the average of these relaxation times (Table 1). Figure 4 shows d_z as a function of time for six representative trajectories for each species. The relaxation time scale is approximately the same for both MUS and MeS, indicating that ΔG_{flip} determines the difference in flipping/translocation time scale.

Using the values of k_d^{-1} and ΔG_{flip} from Table 1, τ_{flip} is estimated for each species using eq 1 and eq 2. τ_{flip} is estimated as 2.4×10^5 s for MeS, or approximately 67 h. Experimental estimates of lipid flip-flop and isolated ion bilayer translocation measure time scales on the order of minutes to tens of hours,^{6,33,35} in reasonable agreement with these calculations. Strikingly, τ_{flip} is estimated as only 1.1 s for the NP-grafted MUS ligand, a 200,000-fold decrease relative to MeS due to the 7.6 kcal/mol decrease in the corresponding value of ΔG_{flip} . These calculations confirm that MUS ligands can flip across the bilayer on biologically relevant time scales.

2.6. OmpLA-Grafted EArg Also Exhibits Reduced Flipping Free Energy Barrier, Increased Flipping Rate. The comparison of the NP-DOPC and MeS-DOPC systems indicates that the time scale for flipping MUS ligands is significantly faster than the time scale for translocating isolated ions because the NP-grafted MUS end group cannot reach bulk water. In principle, other systems in which a charged group is

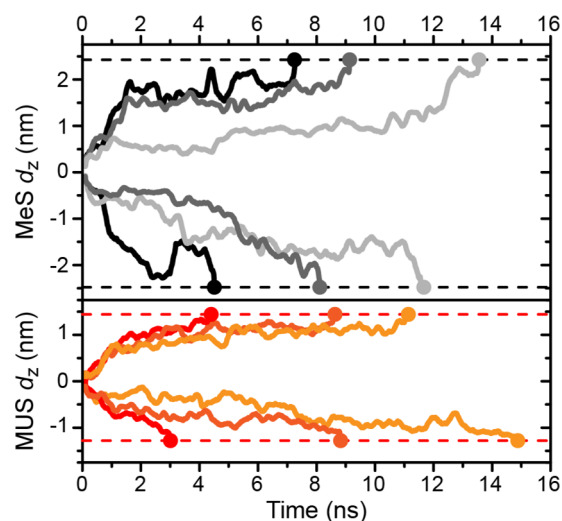


Figure 4. Unbiased relaxation of charged species from the center of the bilayer ($d_z = 0$) to local free energy minima. The plots show d_z as a function of time for six example MeS trajectories (shades of black, at top) and six example MUS trajectories (shades of red, at bottom). Values of d_z corresponding to local minima in the PMFs in Figure 2 are indicated with horizontal dashed lines. The points indicate the times at which the charged species reach local minima in each trajectory and are used to calculate k_d^{-1} (Table 1). Different shades are only to visually distinguish independent trajectories.

grafted to a membrane-embedded scaffold could also exhibit a low flipping barrier. To test the generality of this finding, we calculate the PMF for flipping an extended arginine variant (EArg) grafted to a β -barrel protein, OmpLA, embedded within a POPC bilayer. This system generalizes the findings to (i) a biologically relevant membrane-embedded scaffold, (ii) a cationic, as opposed to anionic, charged species, (iii) a different lipid composition, and (iv) a different molecular force field (see Methods). OmpLA is a suitable protein scaffold because of its stability in the membrane²⁷ and prior usage in the derivation of biological hydrophobicity scales.²⁵ While a single α -helix could be used, the ability of a single helix to tilt or translate vertically relative to the membrane could reduce the effect of the scaffold.^{5,26,36} EArg is used to compare with the similarly sized MUS ligand and does not represent a specific physical system.

Figure 5 compares the PMF for flipping OmpLA-grafted EArg to the PMF for translocating an isolated MGuan molecule as a function of d_z . For these calculations, d_z is defined as the distance, projected onto the z -axis, between the center of mass of the lipid bilayer and the carbon atom in the guanidinium group. The MGuan PMF is symmetric and resembles the PMF for MeS (Figure 2). ΔG_{flip} for MGuan is 14.4 kcal/mol, which is less than ΔG_{flip} for MeS; this difference is expected due to known variations in the values calculated with different lipid compositions³⁷ and molecular force fields.³⁸ Unlike the rest of the PMFs, the EArg PMF is highly asymmetric, with a difference of approximately 5 kcal/mol between the two minima. Given this asymmetry, separate values of ΔG_{flip} are determined for EArg relative to each minimum (Table 1). Both values of ΔG_{flip} for EArg are less than ΔG_{flip} for MGuan; the smaller value of ΔG_{flip} is 7.2 kcal/mol less than ΔG_{flip} for MGuan, which is comparable to the difference in ΔG_{flip} between MUS and MeS. Table 1 shows values of τ_{flip} calculated in the same manner as with the MUS and MeS systems (example relaxation trajectories analogous to Figure 4 are

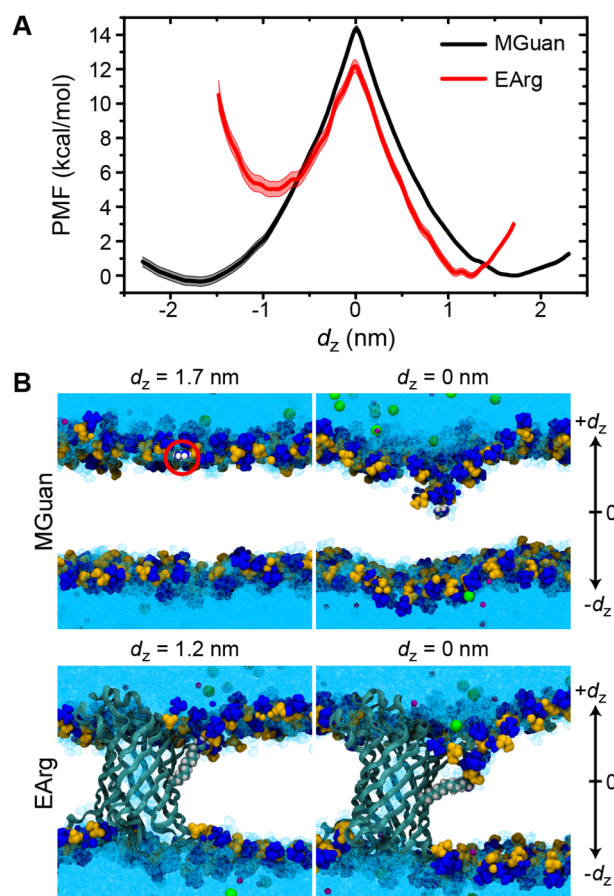


Figure 5. Free energy cost for translocating MGuan and flipping EArg across the bilayer. (A) PMFs for translocating an isolated MGuan molecule (black) and flipping an OmpLA-grafted EArg residue (red) as a function of d_z . Each PMF curve is offset such that its minimum value for $d_z \gg 0.0$ is set to zero. The error is shown as the shaded region around each solid line. (B) Representative snapshots of the configurations at the minimum (for $d_z \gg 0$) and maximum of both the MGuan and EArg PMFs. The OmpLA backbone is shown in the “ribbon” representation.

presented in Figure S4). The translocation time scale, τ_{flip} , for MGuan is on the order of a minute, again in reasonable agreement with experiments,^{6,33,35} while both EArg flipping time scales occur significantly more rapidly on the millisecond to second time scale. These results confirm that grafting a charged species to a membrane-embedded scaffold increases its flipping rate, independent of the exact system composition.

2.7. Interactions between EArg and OmpLA Residues Account for Asymmetry in Flipping PMF. A significant difference between the OmpLA scaffold and NP scaffold is the asymmetric distribution of polar and aromatic OmpLA amino acid side chains that are accessible from within the membrane core. Visual inspection of the US trajectories clearly identifies interactions between EArg and OmpLA side chains for $d_z < 0$, hinting at the origin of the asymmetry in Figure 5. Figure 6A presents snapshots of representative interactions, including a hydrogen bond formed between the EArg end group and an asparagine residue (at left) and a cation– π interaction between the EArg end group and an tryptophan residue (at right).

To quantify the effect of these interactions, Figure 6 presents the coordination number (N_{coord}) of EArg as defined previously (see Figure 3) but modified to account for interactions with

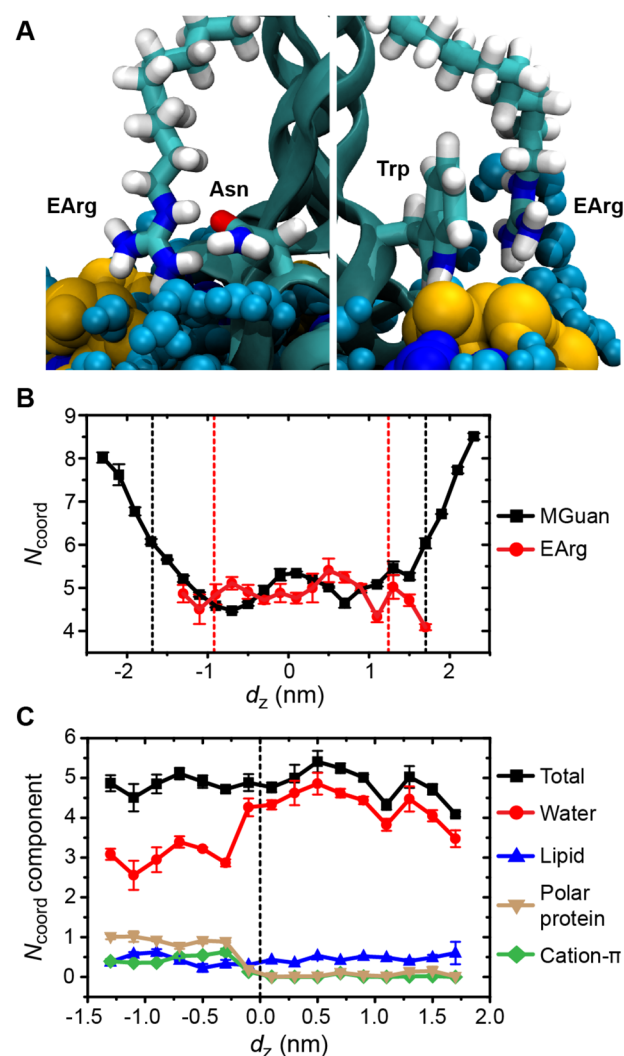


Figure 6. Analysis of EArg interactions. (A) Snapshots of interactions between EArg and other OmpLA side chains, including a hydrogen bond formed with Asn (at left) and a cation– π interaction formed with Trp (at right). Side chains are shown in a “licorice” representation to emphasize their relative orientations. Water molecules (cyan) are shown in a space-filling representation to illustrate interactions with EArg. Both snapshots are taken for a configuration in which $d_z = -0.4$ nm. (B) N_{coord} , the number of polar groups coordinating each species. N_{coord} for EArg includes contributions from OmpLA side chains. Dashed lines indicate the positions of the MGuan (black) and EArg (red) minima from the PMFs in Figure 5. (C) N_{coord} for EArg split into different contributions. The dashed vertical line emphasizes the asymmetry in protein interactions with respect to $d_z = 0$.

polar and aromatic side chains. A polar side chain is counted as coordinating EArg if at least one atom with a charge greater than 0.5 or less than -0.5 is within 0.5 nm of the central carbon of the EArg guanidinium group. A cation– π interaction with an aromatic side chain is counted if the center of mass of the six-membered ring in tryptophan, tyrosine, or phenylalanine is within 0.45 nm of the central carbon atom of the EArg guanidinium group, which is sufficient to identify the favorable “stacked” arrangement frequently observed in membrane proteins^{39–41} (illustrated in Figure 6A).

Figure 6B compares N_{coord} for MGuan and EArg in analogy to Figure 3C, and again shows that the grafted species has a decreased coordination number throughout the entire range of d_z values sampled in Figure 5. Figure 6C shows N_{coord} split into

interactions with water, lipids, polar protein side chains, and cation- π interactions (counterions do not coordinate EArg for any value of d_z). While the total value of N_{coord} is invariant with respect to d_z , there is an increase in interactions with OmpLA side chains for $d_z < 0$, leading to a decrease in water coordination.

These protein interactions explain the lower value of ΔG_{flip} for $d_z < 0$. First, coordination by a protein side chain is more favorable than coordination by water because it does not require the penetration of a water molecule into the hydrophobic membrane core. This difference is apparent from the snapshots in Figure 6A; the snapshot on the right shows an intramembrane water molecule interacting with the EArg end group in place of the asparagine residue shown in the snapshot on the left. This finding agrees with prior work in which a lower barrier for translocating a guanidinium ion was calculated when the ion was positioned near transmembrane α -helices due to interactions with the helix backbones.⁴² Second, cation- π interactions provide significant intramembrane stability while still allowing the EArg end group to form its typical number of hydrogen bonds.^{40,41,43} Both effects combine to stabilize unfavorable intermediate states along the flipping pathway and lower the ΔG_{flip} for EArg relative to its minimum for $d_z < 0$. These results illustrate another effect of grafting: attaching the charged species to the protein backbone enables interactions with side chains and other polar groups that reduce the flipping barrier.

3. DISCUSSION

3.1. Rapid MUS Flipping Time Scale Explains Experimental Observations of NP-Bilayer Insertion.

Prior experimental observations have found that small, charged NPs can insert into lipid bilayers nondisruptively,^{17,18} despite the large free energy barrier that inhibits the passive diffusion of charged species across the hydrophobic bilayer core. Insertion correlates with an increase in nonendocytic cell uptake.¹⁸ Building upon prior studies,^{18,20,44–47} the results of this work support a pathway in which amphiphilic NPs insert into lipid bilayers via the iterative, stepwise flipping of charged ligands across the bilayer. Consistent with the experimental results, the PMF calculations (Figure 2) confirm that the flipping free energy barrier and corresponding time scale are significantly lower for NP-grafted charged ligands than for isolated ions, indicating that ligand flipping is possible on physiologically relevant time scales. The flipping process induces local lipid deformations as opposed to forming a membrane-spanning pore (Figure 3), which is again consistent with the experimental finding that NP insertion does not allow the passage of a membrane-impermeable dye.¹⁸ Figure 3 indicates that the free energy barrier for flipping NP-grafted ligands is reduced because the ligand end group is confined near the membrane interface and cannot reach bulk water. The free energy penalty for this dehydration is thus compensated for by the favorable hydrophobic interactions that drive the initial insertion of the amphiphilic NP into the bilayer.^{20,44,45,47} While these simulations only consider a membrane-embedded NP with a symmetric transmembrane ligand distribution, the insertion of the NP into a single bilayer leaflet still leaves ligands in highly strained states consistent with the configurations shown in Figure 2,⁴⁷ indicating that ligands would face a similar flipping free energy barrier for other ligand distributions. We note that a recent study by Simonelli et al. identified a similar pathway for bilayer insertion that also involves charged ligands flipping

across the bilayer.⁴⁸ While the authors did not describe the molecular details of the flipping process and the reported flipping barrier (≈ 5 kcal/mol) is likely underestimated due to the use of a coarse-grained molecular force field,⁴⁸ their results are in qualitative agreement with this study.

In this work, we study only single-component DOPC or POPC bilayers to replicate prior experiments using synthetic lipid vesicles,¹⁸ while cell membranes contain many lipid species (including saturated lipids of varying lengths) and other components that may affect the measured energy barriers. However, given prior correlations between bilayer interactions in synthetic systems and nonendocytic cellular uptake,¹⁸ we expect that any such change in composition may modify the quantitative flipping rates measured experimentally, but would preserve the identified trend that grafted ligands cross the membrane significantly more rapidly than isolated ions.

3.2. Implications for Material Design. This work has several implications relevant to the design of NPs capable of rapidly flipping ligands across lipid bilayers. These simulations predict that longer ligands should have a larger flipping barrier than shorter ligands because they can more easily access bulk water, even when grafted to the NP core. In previous work,⁴⁴ the free energy change for embedding NPs grafted with end-functionalized ligands containing fewer than eight methylene groups was found to be unfavorable. Combined, these two results suggest that there is an optimal ligand length for which embedding is favorable and flipping occurs rapidly. For a DOPC bilayer, for which both results were computed, ligands should contain on the order of 9–11 methylene groups such that ligands are slightly shorter than half the bilayer thickness (slightly thinning the bilayer, as observed previously⁴⁶); thinner or thicker bilayers would require shorter or longer ligands, respectively. The flipping barrier may also increase if the entire NP core can rotate or translate relative to the membrane to increase end group solvent exposure. The EArg simulations further demonstrate that interactions with other molecules grafted to the membrane-embedded scaffold can enhance flipping, suggesting that aromatic molecules could be incorporated into the NP surface monolayer to mimic the cation- π interactions that stabilize OmpLA-grafted EArg flipping. Finally, flipping induces local bilayer defects that should enable the cooperative transfer of multiple charged species simultaneously,^{49,50} which may allow ligands to be functionalized with multiple charged groups that flip as a single species. Future studies will focus on defining similar design rules to identify optimal ligand and NP surface properties based on the fundamental insight provided in this work.

3.3. Relevance for Biological Systems. Past work has suggested that charge translocation in biological systems is sensitive to a number of factors, including bilayer thickness,⁵¹ bilayer phase behavior,⁵² or the presence of transmembrane helices.^{42,53} The study of the OmpLA-grafted EArg system suggests that grafting charged species to a membrane-embedded scaffold also increases the rate of charge translocation and may be relevant to biological macromolecules. For example, some membrane proteins have individual charged side chains that strongly deform the surrounding bilayer, leading to local hydrophobic mismatch.⁵⁴ These findings suggest that such residues may readily flip-flop across the membrane, which could be relevant to protein function. Moreover, the lower barrier for flipping depends primarily on the restricted solvent accessibility of the charged group, which may also affect the translocation of membrane protein loops that are constrained near the bilayer

interface. Indeed, the surprising translocation of highly charged soluble loops has been reported for several different transmembrane proteins,^{8,10,12} even in the absence of protein chaperones,¹⁵ which may be due to the lower barriers identified here.

The finding that the flipping barrier for EArg is lowered by interactions with side chains on the same protein backbone suggests that membrane proteins can “self-catalyze” charge translocation, which may be important for the spontaneous insertion of proteins that first bind to the membrane interface. For example, the folding and refolding of various bacterial outer membrane proteins in synthetic, neutral, single-component lipid vesicles is kinetically controlled by factors similar to the ones that affect charge translocation, including bilayer thickness⁵⁵ and the presence of bilayer defects,⁵⁶ indicating that folding may require charged or hydrophilic groups to cross the membrane.²⁵ While folding in true biological membranes likely involves factors including membrane asymmetry, protein chaperones, or other membrane components such as lipopolysaccharides,^{57,58} the results of this work support the hypothesis that spontaneous membrane protein folding may also be accelerated by cooperative interaction between side chains that facilitates the transfer of charged groups across the membrane. In this respect, future work will be needed to determine these folding pathways.

4. CONCLUSIONS

In this work, we use atomistic molecular dynamics simulations to quantify the free energy barrier for flipping a charged species across a lipid bilayer, and specifically focus on understanding the effect of grafting the charged species to a membrane-embedded scaffold. We find that the free energy barrier for flipping a charged ligand grafted to a membrane-embedded NP is over 7 kcal/mol lower than the barrier for flipping an isolated analogue to the end group, leading to a 200,000-fold decrease in the corresponding flipping time scale. Flipping induces localized defects in the bilayer, as opposed to large pores, agreeing with prior experiments.^{17,18} The free energy barrier is lower for the NP-grafted ligand because the end group is poorly solvated in its equilibrium configuration and does not have to further dehydrate when crossing the bilayer. To generalize this finding to a biologically relevant scaffold, the same calculations are repeated for an extended arginine variant grafted to a membrane-embedded β -barrel protein. It is again found that the flipping time scale is significantly faster for the grafted species, with additional stability in this case conferred by interactions between the charged species and other amino acid side chains. These results confirm that charged species grafted to both synthetic and biological membrane-embedded scaffolds can flip across lipid bilayers significantly faster than anticipated, yielding mechanistic insight into the translocation of charged membrane protein loops and highly charged monolayer-protected nanoparticles.

5. METHODS

The four systems simulated in this work are summarized in Figure 1. The NP-DOPC system contains 334 lipids, while the MeS-DOPC system contains 200; the larger NP-DOPC bilayer size ensures that lipid deformations around the NP relax by the edge of the periodic simulation cell.⁴⁶ Both systems are solvated in an electroneutral 150 mM NaCl solution. The OmpLA-POPC system contains 202 lipids to match previous simulation

studies,²⁶ while the MGuan-POPC system contains 200 lipids. Both systems are solvated in an electroneutral 150 mM NaCl solution. Methods for preparing all four simulated systems are summarized in the Supporting Information and Figure S1.

Molecular dynamics is performed for all systems with a simulation time step of 2 fs, a constant temperature of 310 K, and a constant pressure of 1 bar. The NP-DOPC and MeS-DOPC system components are modeled using the GROMOS 54a7 united-atom force field with the SPC water model.^{59,60} Parameters for the gold core, MUS, and OT are taken from previous work.⁶¹ The OmpLA-POPC and MGuan-POPC system components are modeled using the CHARMM36 all-atom force field with the TIP3P water model.^{62,63} Parameters for the extended alkyl backbone of EArg are adapted from existing parameters for saturated lipid tails.⁶⁴ Simulations of the NP-DOPC and MeS-DOPC systems are performed using version 4.6.7 of the Gromacs simulation package, while simulations of the OmpLA-POPC and MGuan-POPC systems are performed using version 5.0.7 of Gromacs.⁶⁵ Complete details on force field and simulation parameters are provided in the Supporting Information.

The potential of mean force (PMF) for transporting each charged species across the bilayer is calculated using an umbrella sampling (US) protocol. The US reaction coordinate, d_z , is defined as the distance, projected onto the z -axis, between the center of mass of the lipid bilayer and either the sulfur atom in the sulfonate group (for MUS and MeS) or the carbon atom in the guanidinium group (for EArg and MGuan). Each system is first equilibrated with unbiased molecular dynamics for at least 50 ns (see Table S3), and then configurations with values of d_z separated by 0.1 nm are generated by pulling each species across the bilayer. For the NP-DOPC system, the MUS end group with the smallest average value of d_z during equilibration is selected to be pulled; no constraint is placed on the NP to prevent rotation during pulling, although in practice rotation is limited by the other charged end groups. Configurations are selected such that only the bilayer leaflet nearest the charged species is deformed to correctly sample low-energy configurations,^{5,6} as discussed in the Supporting Information and Figure S5. Two configurations, one in which each leaflet is deformed, are generated for $d_z = 0$.⁶ A 70 ns US trajectory is initialized from each configuration with the species restrained to the desired value of d_z using an umbrella potential with a spring constant of 1000 kJ/mol/nm². The first 10 ns of each US trajectory is discarded as equilibration, and the PMF is calculated from the remaining data using the weighted histogram analysis method.⁶⁶ This sampling time is sufficient to obtain convergence (Figure S6). Error bars are computed from statistical bootstrapping of the US histograms using the program *g_wham*.⁶⁷ Additional details on the US workflow are included in the Supporting Information.

■ ASSOCIATED CONTENT

§ Supporting Information

The Supporting Information is available free of charge on the ACS Publications website at DOI: 10.1021/acscentsci.6b00365.

Full model and force field details, description of system preparation and umbrella sampling workflow, summary of system components and simulations performed, and additional figures (PDF)

AUTHOR INFORMATION

Corresponding Author

*E-mail: vanlehn@wisc.edu.

ORCID

Reid C. Van Lehn: 0000-0003-4885-6599

Notes

The authors declare no competing financial interest.

ACKNOWLEDGMENTS

R.C.V.L. and A.A.-K. acknowledge support by the MRSEC Program of the National Science Foundation under Award No. DMR-0819762 and from NSF CAREER Award No. DMR-1054671. The simulations in this work used the Extreme Science and Engineering Discovery Environment (XSEDE), which is supported by National Science Foundation Grant No. OCI-1053575.

REFERENCES

- (1) Deamer, D. W.; Bramhall, J. Permeability of lipid bilayers to water and ionic solutes. *Chem. Phys. Lipids* **1986**, *40*, 167–188.
- (2) Rajendran, L.; Knölker, H.-J.; Simons, K. Subcellular targeting strategies for drug design and delivery. *Nat. Rev. Drug Discovery* **2010**, *9*, 29–42.
- (3) Muro, S. Challenges in design and characterization of ligand-targeted drug delivery systems. *J. Controlled Release* **2012**, *164*, 125–137.
- (4) Wilson, M. A.; Pohorille, A. Mechanism of unassisted ion transport across membrane bilayers. *J. Am. Chem. Soc.* **1996**, *118*, 6580–6587.
- (5) Li, L.; Vorobyov, I.; Allen, T. W. Potential of mean force and pKa profile calculation for a lipid membrane-exposed arginine side chain. *J. Phys. Chem. B* **2008**, *112*, 9574–9587.
- (6) Vorobyov, I.; Olson, T.; Kim, J.; Koeppe, R.; Andersen, O.; Allen, T. Ion-induced defect permeation of lipid membranes. *Biophys. J.* **2014**, *106*, 586–597.
- (7) Wang, Y.; Hu, D.; Wei, D. Transmembrane permeation mechanism of charged methyl guanidine. *J. Chem. Theory Comput.* **2014**, *10*, 1717–1726.
- (8) Bowie, J. U. Membrane protein twists and turns. *Science* **2013**, *339*, 398–399.
- (9) Lu, Y.; Turnbull, I. R.; Bragin, A.; Carveth, K.; Verkman, A. S.; Skach, W. R. Reorientation of aquaporin-1 topology during maturation in the endoplasmic reticulum. *Mol. Biol. Cell* **2000**, *11*, 2973–2985.
- (10) Virkki, M. T.; Agrawal, N.; Edsbäcker, E.; Cristobal, S.; Elofsson, A.; Kauko, A. Folding of aquaporin 1: Multiple evidence that helix 3 can shift out of the membrane core. *Protein Sci.* **2014**, *23*, 981–992.
- (11) Seppälä, S.; Slusky, J. S.; Lloris-Garcera, P.; Rapp, M.; von Heijne, G. Control of membrane protein topology by a single C-terminal residue. *Science* **2010**, *328*, 1698–1700.
- (12) Van Lehn, R. C.; Zhang, B.; Miller, T. F. Regulation of multispinning membrane protein topology via post-translational annealing. *eLife* **2015**, *4*, 1–23.
- (13) Woodall, N. B.; Yin, Y.; Bowie, J. U. Dual-topology insertion of a dual-topology membrane protein. *Nat. Commun.* **2015**, *6*, 1–8.
- (14) Bogdanov, M.; Xie, J.; Heacock, P.; Dowhan, W. To flip or not to flip: Lipid-protein charge interactions are a determinant of final membrane protein topology. *J. Cell Biol.* **2008**, *182*, 925–935.
- (15) Vitrac, H.; Bogdanov, M.; Dowhan, W. In vitro reconstitution of lipid-dependent dual topology and postassembly topological switching of a membrane protein. *Proc. Natl. Acad. Sci. U. S. A.* **2013**, *110*, 9338–9343.
- (16) Vitrac, H.; MacLean, D. M.; Jayaraman, V.; Bogdanov, M.; Dowhan, W. Dynamic membrane protein topological switching upon changes in phospholipid environment. *Proc. Natl. Acad. Sci. U. S. A.* **2015**, *112*, 13874–13879.
- (17) Verma, A.; Uzun, O.; Hu, Y. Y.; Han, H.-S.; Watson, N.; Chen, S.; Irvine, D. J.; Stellacci, F. Surface-structure-regulated cell-membrane penetration by monolayer-protected nanoparticles. *Nat. Mater.* **2008**, *7*, 588–595.
- (18) Van Lehn, R. C.; Atukorale, P. U.; Carney, R. P.; Yang, Y.-S.; Stellacci, F.; Irvine, D. J.; Alexander-Katz, A. Effect of particle diameter and surface composition on the spontaneous fusion of monolayer-protected gold nanoparticles with lipid bilayers. *Nano Lett.* **2013**, *13*, 4060–4067.
- (19) Carney, R. P.; Astier, Y.; Carney, T. M.; Voitchovsky, K.; Jacob Silva, P. H.; Stellacci, F. Electrical method to quantify nanoparticle interaction with lipid bilayers. *ACS Nano* **2013**, *7*, 932–942.
- (20) Van Lehn, R. C.; Ricci, M.; Silva, P. H. J.; Andreozzi, P.; Reguera, J.; Voitchovsky, K.; Stellacci, F.; Alexander-Katz, A. Lipid tail protrusions mediate the insertion of nanoparticles into model cell membranes. *Nat. Commun.* **2014**, *5*, 1–11.
- (21) Atukorale, P. U.; Yang, Y.-S.; Bekdemir, A.; Carney, R. P.; Silva, P. J.; Watson, N.; Stellacci, F.; Irvine, D. J. Influence of the glycocalyx and plasma membrane composition on amphiphilic gold nanoparticle association with erythrocytes. *Nanoscale* **2015**, *7*, 11420–11432.
- (22) Lee, H.-Y.; Shin, S. H. R.; Abezgauz, L. L.; Lewis, S. A.; Chirsan, A. M.; Danino, D. D.; Bishop, K. J. M. Integration of gold nanoparticles into bilayer structures via adaptive surface chemistry. *J. Am. Chem. Soc.* **2013**, *135*, 5950–5953.
- (23) Tatur, S.; Maccarini, M.; Barker, R.; Nelson, A.; Fragneto, G. Effect of functionalized gold nanoparticles on floating lipid bilayers. *Langmuir* **2013**, *29*, 6606–6614.
- (24) Gordillo, G. J.; Krpetić, Z.; Brust, M. Interactions of gold nanoparticles with a phospholipid monolayer membrane on mercury. *ACS Nano* **2014**, *8*, 6074–6080.
- (25) Moon, C. P.; Fleming, K. G. Side-chain hydrophobicity scale derived from transmembrane protein folding into lipid bilayers. *Proc. Natl. Acad. Sci. U. S. A.* **2011**, *108*, 25–28.
- (26) Gumbart, J.; Roux, B. Determination of membrane-insertion free energies by molecular dynamics simulations. *Biophys. J.* **2012**, *102*, 795–801.
- (27) Fleming, P. J.; Freitas, J. A.; Moon, C. P.; Tobias, D. J.; Fleming, K. G. Outer membrane phospholipase A in phospholipid bilayers: A model system for concerted computational and experimental investigations of amino acid side chain partitioning into lipid bilayers. *Biochim. Biophys. Acta, Biomembr.* **2012**, *1818*, 126–134.
- (28) Neale, C.; Madill, C.; Rauscher, S.; Pomès, R. Accelerating convergence in molecular dynamics simulations of solutes in lipid membranes by conducting a random walk along the bilayer normal. *J. Chem. Theory Comput.* **2013**, *9*, 3686–3703.
- (29) Sapay, N.; Bennett, W. F. D.; Tieleman, D. P. Thermodynamics of flip-flop and desorption for a systematic series of phosphatidylcholine lipids. *Soft Matter* **2009**, *5*, 3295.
- (30) Qiao, B.; Olvera de la Cruz, M. Driving force for water permeation across lipid membranes. *J. Phys. Chem. Lett.* **2013**, *4*, 3233–3237.
- (31) Jo, S.; Rui, H.; Lim, J. B.; Klauda, J. B.; Im, W. Cholesterol flip-flop: insights from free energy simulation studies. *J. Phys. Chem. B* **2010**, *114*, 13342–13348.
- (32) Maccallum, J. L.; Bennett, W. F. D.; Tieleman, D. P. Distribution of amino acids in a lipid bilayer from computer simulations. *Biophys. J.* **2008**, *94*, 3393–404.
- (33) Tieleman, D. P.; Marrink, S.-J. Lipids out of equilibrium: energetics of desorption and pore mediated flip-flop. *J. Am. Chem. Soc.* **2006**, *128*, 12462–12467.
- (34) Sapay, N.; Bennett, W. F. D.; Tieleman, D. P. Molecular simulations of lipid flip-flop in the presence of model transmembrane helices. *Biochemistry* **2010**, *49*, 7665–7673.
- (35) Wheaten, S. A.; Ablan, F. D. O.; Spaller, B. L.; Trieu, J. M.; Almeida, P. F. Translocation of cationic amphipathic peptides across the membranes of pure phospholipid giant vesicles. *J. Am. Chem. Soc.* **2013**, *135*, 16517–16525.
- (36) Schow, E. V.; Freitas, J. A.; Cheng, P.; Bernsel, A.; von Heijne, G.; White, S. H.; Tobias, D. J. Arginine in membranes: the connection

between molecular dynamics simulations and translocon-mediated insertion experiments. *J. Membr. Biol.* **2011**, 239, 35–48.

(37) Johansson, A. C. V.; Lindahl, E. The role of lipid composition for insertion and stabilization of amino acids in membranes. *J. Chem. Phys.* **2009**, 130, 185101.

(38) Sun, D.; Forsman, J.; Woodward, C. E. Evaluating force fields for the computational prediction of ionized arginine and lysine side-chains partitioning into lipid bilayers and octanol. *J. Chem. Theory Comput.* **2015**, 11, 1775–1791.

(39) Flocco, M. M.; Mowbray, S. L. Planar stacking interactions of arginine and aromatic side-chains in proteins. *J. Mol. Biol.* **1994**, 235, 709–717.

(40) Minoux, H.; Chipot, C. Cation- π interactions in proteins: Can simple models provide an accurate description? *J. Am. Chem. Soc.* **1999**, 121, 10366–10372.

(41) Gallivan, J. P.; Dougherty, D. A. Cation- π interactions in structural biology. *Proc. Natl. Acad. Sci. U. S. A.* **1999**, 96, 9459–9464.

(42) Johansson, A. C. V.; Lindahl, E. Protein contents in biological membranes can explain abnormal solvation of charged and polar residues. *Proc. Natl. Acad. Sci. U. S. A.* **2009**, 106, 15684–15689.

(43) Crowley, P. B.; Golovin, A. Cation- π Interactions in protein-protein interfaces. *Proteins: Struct., Funct., Genet.* **2005**, 59, 231–239.

(44) Van Lehn, R. C.; Alexander-Katz, A. Free energy change for insertion of charged, monolayer-protected nanoparticles into lipid bilayers. *Soft Matter* **2014**, 10, 648–658.

(45) Van Lehn, R. C.; Alexander-Katz, A. Fusion of ligand-coated nanoparticles with lipid bilayers: Effect of ligand flexibility. *J. Phys. Chem. A* **2014**, 118, 5848–5856.

(46) Van Lehn, R. C.; Alexander-Katz, A. Membrane-embedded nanoparticles induce lipid rearrangements similar to those exhibited by biological membrane proteins. *J. Phys. Chem. B* **2014**, 118, 12586–12598.

(47) Van Lehn, R. C.; Alexander-Katz, A. Pathway for insertion of amphiphilic nanoparticles into defect-free lipid bilayers from atomistic molecular dynamics simulations. *Soft Matter* **2015**, 11, 3165–3175.

(48) Simonelli, F.; Bochicchio, D.; Ferrando, R.; Rossi, G. Monolayer-protected anionic Au nanoparticles walk into lipid membranes step by step. *J. Phys. Chem. Lett.* **2015**, 6, 3175–3179.

(49) MacCallum, J. L.; Bennett, W. F. D.; Tieleman, D. P. Transfer of arginine into lipid bilayers is nonadditive. *Biophys. J.* **2011**, 101, 110–117.

(50) Allolio, C.; Baxova, K.; Vazdar, M.; Jungwirth, P. Guanidinium pairing facilitates membrane translocation. *J. Phys. Chem. B* **2016**, 120, 143–153.

(51) Li, L. B.; Vorobyov, I.; Allen, T. W. The role of membrane thickness in charged protein-lipid interactions. *Biochim. Biophys. Acta, Biomembr.* **2012**, 1818, 135–145.

(52) John, K.; Schreiber, S.; Kubelt, J.; Herrmann, A.; Müller, P. Transbilayer movement of phospholipids at the main phase transition of lipid membranes: implications for rapid flip-flop in biological membranes. *Biophys. J.* **2002**, 83, 3315–3323.

(53) Anglin, T. C.; Liu, J.; Conboy, J. C. Facile lipid flip-flop in a phospholipid bilayer induced by gramicidin A measured by sum-frequency vibrational spectroscopy. *Biophys. J.* **2007**, 92, L01–L03.

(54) Mondal, S.; Khelashvili, G.; Shi, L.; Weinstein, H. The cost of living in the membrane: A case study of hydrophobic mismatch for the multi-segment protein LeuT. *Chem. Phys. Lipids* **2013**, 169, 27–38.

(55) Burgess, N. K.; Dao, T. P.; Stanley, A. M.; Fleming, K. G. β -Barrel proteins that reside in the Escherichia coli outer membrane in vivo demonstrate varied folding behavior in vitro. *J. Biol. Chem.* **2008**, 283, 26748–26758.

(56) Danoff, E. J.; Fleming, K. G. Membrane defects accelerate outer membrane β -barrel protein folding. *Biochemistry* **2015**, 54, 97–99.

(57) Tamm, L. K.; Hong, H.; Liang, B. Folding and assembly of β -barrel membrane proteins. *Biochim. Biophys. Acta, Biomembr.* **2004**, 1666, 250–263.

(58) Ruiz, N.; Kahne, D.; Silhavy, T. J. Advances in understanding bacterial outer-membrane biogenesis. *Nat. Rev. Microbiol.* **2006**, 4, 57–66.

(59) Oostenbrink, C.; Villa, A.; Mark, A. E.; van Gunsteren, W. F. A biomolecular force field based on the free enthalpy of hydration and solvation: the GROMOS force-field parameter sets 53A5 and 53A6. *J. Comput. Chem.* **2004**, 25, 1656–1676.

(60) Poger, D.; Mark, A. E. Lipid bilayers: the effect of force field on ordering and dynamics. *J. Chem. Theory Comput.* **2012**, 8, 4807–4817.

(61) Van Lehn, R. C.; Alexander-Katz, A. Structure of mixed-monolayer-protected nanoparticles in aqueous salt solution from atomistic molecular dynamics simulations. *J. Phys. Chem. C* **2013**, 117, 20104–20115.

(62) Best, R. B.; Zhu, X.; Shim, J.; Lopes, P. E. M.; Mittal, J.; Feig, M.; MacKerell, A. D. Optimization of the additive CHARMM all-atom protein force field targeting improved sampling of the backbone ϕ , ψ and side-chain χ 1 and χ 2 Dihedral Angles. *J. Chem. Theory Comput.* **2012**, 8, 3257–3273.

(63) Huang, J.; Mackerell, A. D. CHARMM36 all-atom additive protein force field: Validation based on comparison to NMR data. *J. Comput. Chem.* **2013**, 34, 2135–2145.

(64) Klauda, J. B.; Venable, R. M.; Freites, J. A.; O'Connor, J. W.; Tobias, D. J.; Mondragon-Ramirez, C.; Vorobyov, I.; MacKerell, A. D.; Pastor, R. W. Update of the CHARMM all-atom additive force field for lipids: validation on six lipid types. *J. Phys. Chem. B* **2010**, 114, 7830–7843.

(65) Pronk, S.; Páll, S.; Schulz, R.; Larsson, P.; Bjelkmar, P.; Apostolov, R.; Shirts, M. R.; Smith, J. C.; Kasson, P. M.; van der Spoel, D.; Hess, B.; Lindahl, E. GROMACS 4.5: A high-throughput and highly parallel open source molecular simulation toolkit. *Bioinformatics* **2013**, 29, 845–854.

(66) Kumar, S.; Rosenberg, J. M.; Bouzida, D.; Swendsen, R. H.; Kollman, P. A. The weighted histogram analysis method for free-energy calculations on biomolecules. I. The method. *J. Comput. Chem.* **1992**, 13, 1011–1021.

(67) Hub, J. S.; de Groot, B. L.; van der Spoel, D. g_wham - a free Weighted Histogram Analysis implementation including robust error and autocorrelation estimates. *J. Chem. Theory Comput.* **2010**, 6, 3713–3720.